Bioenerg. Res. (2014) 7:1541–1549
DOI 10.1007/s12155-014-9492-y

Dominated Effect Analysis of the Channel Size of Silica Support Materials on the Catalytic Performance of Immobilized Lipase Catalysts in the Transformation of Unrefined Waste Cooking Oil to Biodiesel

Haidong Zhang · Yu Zou · Yu Shen · Xue Gao · Xuxu Zheng · Xianming Zhang · Youpeng Chen · Jinsong Guo

Published online: 24 June 2014

Abstract Three mesoporous silica materials with various channel sizes and structures were employed to prepare immobilized lipase catalysts for the transesterification of unrefined wasted cooking oil (UWCO) to biodiesel at room temperature. The channel size of support material was found to be the key point to obtain high initial specific activity and high sustainability of activity of the immobilized lipase catalysts. A SBA-15 material with appropriate channel size (14.0 nm) demonstrates the best capacity of lipase. The immobilized catalyst with the SBA-15 material shows much higher activity and sustainability of activity than the immobilized catalysts with a MCM-41 material (channel size 1.8 nm) and a mesostructured cellular foam (MCF) material (channel size 28.0 nm) as support materials in the transformation of UWCO to biodiesel. After 60 h of reaction at 28 °C, a fatty acid methyl ester (FAME) yield up to 80.1 and 71.8 % of initial specific activity can be achieved using SBA-15-immobilized lipase.

Keywords Immobilized lipase · Channel size · Biodiesel · Waste cooking oil · Mesoporous silica materials

H. Zhang (✉) · Y. Zou · Y. Shen · X. Gao · X. Zheng · X. Zhang
Engineering Research Centre for Wasted Oil Recovery Technology of Chinese Ministry of Education, Chongqing Key Laboratory of Catalysis Science and Technology, School of Environmental and Biological Engineering, Chongqing Technology and Business University, Chongqing 400067, China
e-mail: haidongzhang@ctbu.edu.cn

Y. Shen (✉) · Y. Chen · J. Guo
Chongqing Institute of Green and Intelligent Technology, Chinese Academy of Sciences, Chongqing 401122, China
e-mail: shenyu@cigit.ac.cn

Introduction

Biodiesel is one of the alternative fuels to conventional diesel fuel. The most common way to produce biodiesel is the transesterification of biomass oils such as those obtained from palm oil, soybean oil, sunflower, castor oil, and also animal oils and the oils from microbes and microalgae [1–3]. However, a major challenge to biodiesel production from these feedstock materials is the high cost, which can be 75 % above in the biodiesel industry, of raw materials [4]. As a promising alternative raw material for the production of biodiesel, wasted cooking oil (WCO) is much cheaper than the aforementioned raw materials, and consequently, the total manufacturing cost of biodiesel can be significantly reduced [5–8].

In addition, the quantity of WCO generated per year by any country is huge and the disposal of WCO is always problematic [4]. In China, the annual production of WCO was 3.98 million tons in 2012 and will reach 5.77 million tons in 2020 [9]. The use of WCO to produce biodiesel can help to solve the problem of wasted oil disposal with high efficiency and economical prospect. The USA has implemented some new policies to encourage the use of WCO for biodiesel production, with tax abatement up to $306/t for using WCO as feedstock as compared to only $153/t for using soybean oil.

The transesterification of WCO to produce biodiesel can be alkali-catalyzed, acid-catalyzed or enzyme-catalyzed. Each process has its own advantages and disadvantages depending on the undesirable compounds like water and free fatty acid (FFA) in WCO. The alkali-catalyzed and acid-catalyzed processes have received much attention but have to face many problems like pretreatment of raw materials, recovery of glycerol, removal of catalysts, and the energy-intensive nature of the process [10, 11]. Enzyme-catalyzed processes have

demonstrated some advantages over traditional acid-catalyzed or alkali-catalyzed processes, such as no generation of byproducts, easy product recovery, mild reaction condition, and especial insensitivity to residual water and FFA [12, 13].

The immobilization of lipase shows a substantial effect on its catalytic activity and leads to much higher thermal stability and extended life than free lipase, especially when the feedstock has high contents of water and FFA [14–16]. In biocatalysis, the use of ordered mesoporous materials as the support materials of immobilized lipase catalysts is a young and growing but still challenging field with still high demand of new and improved catalysts [17]. Mesoporous silicates have narrow channel size in the range of 20–500 Å and high specific surface area and pore volume, which can benefit the adsorbing or entrapping of large molecules within their nanopores [18]. Diaz and Balkus first immobilized enzymes onto mesoporous MCM-41 [19]. Since then, many factors of mesoporous materials, including the relative size of mesopore and enzyme, surface area, channel size distribution, pore volume and particle size, have been found to show a strong influence on the enzyme loading and on their catalytic activity [20]. Big channel size and short channel length were found to show advantages in the immobilization of enzyme because they can benefit the entrapping of enzyme inside the nano-pores and remarkably reduce the diffusion limitation, especially when the feedstock is a high-impurity material like WCO [21–23]. Part of the immobilization of enzyme still remains an art while it is slowly turning into a well-understood science [24].The systematic study on the effect of different channel sizes and structures of mesoporous silicates on the catalytic behavior of immobilized lipase catalysts is still necessary.

In this study, we report our first attempt at the transformation of unrefined wasted cooking oil (UWCO) to biodiesel catalyzed by the immobilized lipase catalysts on three different mesoporous silica materials, a spherical MCM-41 material, a mesostructured cellular foam (MCF) material, and a non-traditional SBA-15 material. UWCO, as a high-impurity feedstock, was obtained from a restaurant without any advanced pretreatment except the filtration to remove indissoluble impurities and then put into reactions at room temperature. The effects of channel size and structure on the lipase capacities of support materials and the catalytic performance in the transesterification of UWCO to biodiesel catalyzed by these immobilized lipase catalysts were studied.

Materials and Methods

Preparation of Mesoporous Silica Materials

To prepare the SBA-15 support material with non-traditional large channel size and short nano-channels, 5 g of EO_{20}–PO_{70}–EO_{20} (Pluronic P123; Aldrich) was added into 175 ml of aqueous HCl solution (1.2 M). When a clear solution was obtained after 30 min of stirring, *n*-decane (Aladdin Chemistry Co. Ltd.) was added to obtain a mixture with an *n*-decane/P123 molar ratio of 250. The mixture was then stirred overnight. The clear separation of a water-rich layer and a decane-rich layer was achieved within 1 day. The upper decane-rich layer was carefully removed, and then 0.1 g of NH_4F (Aladdin Chemistry Co. Ltd.) was added into the water-rich layer [25, 26]. The water-rich layer was then stirred at 40 °C for 15 min, followed by the addition of tetraethyl orthosilicate (TEOS; Aladdin Chemistry Co. Ltd.), keeping a TEOS/P123 molar ratio of 50. This mixture was refluxed at 40 °C for 24 h and then hydrothermally treated in an autoclave at 100 °C for 60 h. The mixture was then filtered to collect the white solid product, which was washed with copious amounts of water and dried at 60 °C in vacuum. Finally, the white powder was calcined at 600 °C for 4 h in a muffle furnace with the supply of air to obtain SBA-15 support material.

To prepare the MCF support material, 16.67 g of P123 was added into 400 ml of an aqueous HCl solution (1.67 M) under stirring at room temperature [27]. When a clear solution was obtained, 0.1875 g of NH_4F and 12.5 g of trimethyl benzene (Aladdin Chemistry Co. Ltd.) were successively added in. The mixture was stirred at 35 °C for 3 h. Then, 35.53 g of TEOS was added into the mixture. This mixture was refluxed at 35 °C for 20 h and then hydrothermally treated in an autoclave at 100 °C for 48 h. The mixture was then filtered to collect the white solid product, which was washed with copious amounts of water and dried at room temperature. Finally, the white powder was calcined at 540 °C for 4 h in a muffle furnace with the supply of air to obtain MCF support material.

To prepare the spherical MCM-41 support material, 30.0 g of cetyltrimethylammonium bromide (Aladdin Chemistry Co. Ltd.) was dissolved in 600 g of deionized water, followed by the addition of 15.8 g of aqueous ammonia (Aladdin Chemistry Co. Ltd.) and 60.0 g of absolute ethanol (Aladdin Chemistry Co. Ltd.). The solution was then stirred for 15 min at 25 °C. Then, 56.4 g of TEOS was added into the solution at one time. The resulting mixture was stirred at 25 °C for 2 h and then filtrated to obtain white precipitate. This white precipitate was washed with a mixture of H_2O and ethanol and then dried at room temperature for 72 h to obtain white power. This white power was calcined at 550 °C for 4 h in a muffle furnace with the supply of air to obtain MCM-41 support material.

Characterizations of Materials

N_2 adsorption–desorption analysis was done at 77 K on a TriStar 3000 instrument. The specific areas of all materials were calculated by Barrett–Joyner–Halenda (BJH) method, and the channel sizes were calculated according to the desorption branches of N_2 adsorption–desorption isotherms. The

small-angle X-ray diffraction (SXRD) patterns were recorded on a Bruker D8 advance X-ray diffractometer with Cu-Kα radiation. Scanning electron microscope (SEM) and high-resolution scanning electron microscope (HRSEM) tests were carried out on a FEI XL30 instrument. Transmission electron microscope (TEM) images were obtained on a FEI Tecnai 20 Twin instrument. Fourier transform infrared spectroscopy (FTIR) spectra and ultraviolet–visible diffuse reflectance spectroscopy (UV–Vis DRS) spectra were recorded on a Shimadzu IRPrestige-21 instrument and a Shimadzu UV-2550 instrument, respectively.

Preparation of Immobilized Lipase Catalysts

The immobilized lipase catalysts were prepared by an incipient wetness impregnation method. Lipase LVK-S200 (used as received from LEVEKING Co. Ltd., Shenzheng, China) was firstly dissolved in a phosphate buffer (pH 5.0). The support materials were then impregnated with this lipase solution for 10 h under mild stirring (50 rpm) and separated through centrifugation after washing twice with phosphate buffer. The solid products were then dried at room temperature in a desiccator for 30 h. After this step in desiccator, the solid products were washed with copious amounts of phosphate buffer to remove the lipase which can be lost by leaching and thus maximally reduce the lipase leaching during transesterification reaction tests. The washed products were dried at room temperature again to achieve the immobilized catalysts and labeled as LVK/SBA-15, LVK/MCF, and LVK/MCM-41, respectively. The initial specific activity of these immobilized lipase catalysts was analyzed by the fatty acid releasing rate of pure olive oil (POO; analytical standard, Supelco). Then, 0.02 g of immobilized catalyst was mixed with 2.0 ml of phosphate buffer (with 10 vol% of POO). The reactant mixture was stirred at 35 °C for 1 h followed by the addition of 4.0 ml of the mixture of ethanol and acetone (ethanol/acetone ratio of 1:1) to terminate the reaction. Four milliliters of 0.02 M NaOH was then added into the mixture. The titration by 0.02 M HCL was then employed to determine the initial specific activity of the catalyst. The unit in the initial specific activity was defined as follows: 1 unit means 1.0 μmol of fatty acid generated/1 min.

Reaction Tests

The WCO used in this study was obtained from a local restaurant, JiaFu Hot Pot. The received WCO was simply filtrated to remove indissoluble impurities to obtain UWCO, which was used as the feedstock for the transesterification reaction. The acid value of filtrated UWCO was 15.8 mg KOH g^{-1}, which was determined by the titration of 0.1 M KOH. In the transesterification reaction tests, UWCO (or POO) and methanol were mixed with a weight ratio of 6:1 (the molecular ratio of methanol to oil was 1:1). The reaction was initiated at room temperature (the temperature in the laboratory was detected by a wet-bulb thermometer and remained at 28 °C with little fluctuation during the reaction tests) under stirring with the addition of immobilized catalyst (0.2 wt% of oil). The total fatty acid methyl ester (FAME) in the reaction medium was detected by a SHIMADZU GC 2010 GC equipped with a FID and a Rtx®-Wax capillary column (30 m, 0.53 mm ID, 0.5 μm). For each injection, a 50:1 split ratio was taken. For each analysis, the GC oven was kept at 200 °C for 4 min and then ramped up to 220 °C within 2 min and then kept at 220 °C for 50 min.

Results and Discussion

Characterizations of Supporting Materials

Figure 1 gives the N_2 adsorption–desorption isotherms of the MCM-41, SBA-15, and MCF support materials. All three support materials exhibit representative type IV isotherms, with typical hysteresis loops of ordered mesoporous materials and narrow size distributions centered at 1.8, 14.0, and 28.2 nm, respectively [28–31]. The textural properties of these three support materials are listed in Table 1. Notably, the channel size of the current SBA-15 material is much larger than that of conventional SBA-15 material. The MCM-41 material shows the biggest specific area but the smallest channel size and pore volume among these three support materials. On the contrary, the MCF material exhibits the smallest specific area but the biggest channel size and pore volume. The SBA-15 material presents medium specific area, channel size, and pore volume.

In the SXRD pattern of the SBA-15 material presented in Fig. 2, four Bragg peaks can be identified between 0.5° and 2.0°, which can be attributed to the (100), (110), (200), and (210) reflections, respectively. The SXRD pattern of the MCM-41 material presents three different Bragg peaks between 2.0° and 6.0°. These peaks are indexed as the (100), (110), and (200) reflections, respectively [29, 31]. The d values calculated by the 2θ values of these Bragg reflections confirm the occurrence of a two-dimensional hexagonal symmetry (p6mm), which is similar to that of MCM-41 and SBA-15 families. Two diffraction peaks at 0.67° and 1.35° can be observed in the SXRD pattern of the MCF material, suggesting a different periodic structure from that of the MCM-41 and SBA-15 materials.

Figure 3 presents the SEM images of these three support materials. We can see that the MCM-41 material exhibits perfectly spherical morphology and most MCM-41 particles are 300–400 nm in diameter. The MCF material shows a typical mesostructure cellar foam structure, which is the same

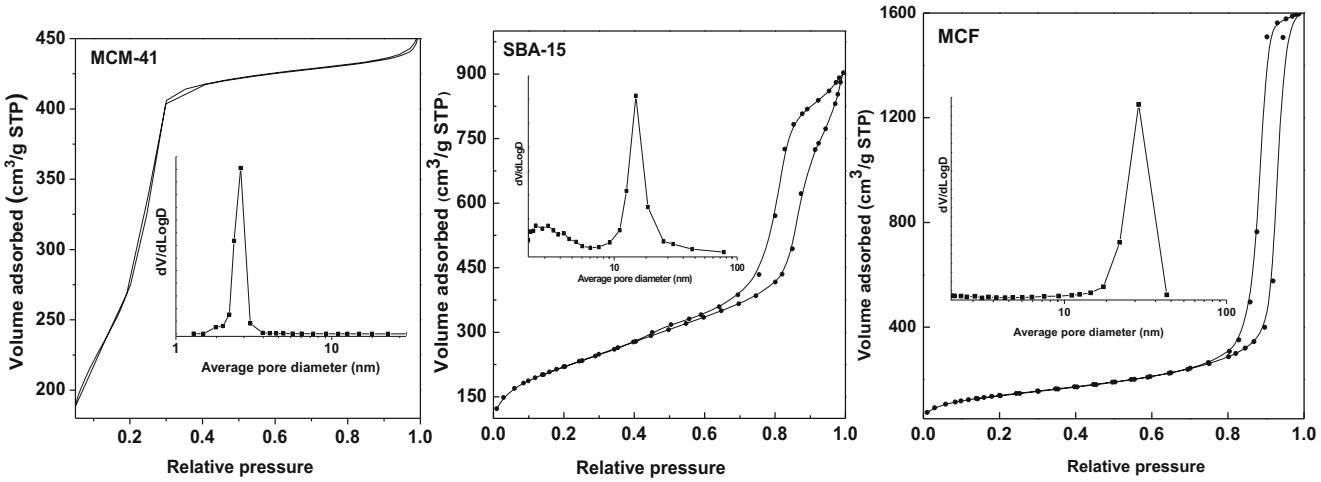

Fig. 1 N_2 adsorption–desorption isotherms of the MCM-41, SBA-15, and MCF support materials. The *insets* are the channel size distribution calculation by the adsorption branches of the adsorption–desorption isotherms

as that reported by Zhao et al. [32]. In the SEM image of the SBA-15 material, we can see that this SBA-15 material presents a unique alternating and bumpy morphology, which is implied by the alternating white and black zones. The HRSEM image in Fig. 3d exhibits that these particles of the SBA-15 material is composed of nano-channels, which are parallelly arranged along the direction being vertical to the long axis of each particle. According to the SXRD pattern of this SBA-15 material, we can know that these nano-channels are hexagonally ordered. The hexagonal symmetry of these nano-channels in the SBA-15 material can also be verified by the TEM images shown in Fig. 4c, d. According to Fig. 4d, we can see that the channel size of this SBA-15 material is around 14 nm, which is in agreement with that calculated by N_2 adsorption–desorption isotherms (Table 1) and much bigger than that of traditional SBA-15 material [27]. Figure 4c suggests that, due to the particle size of this SBA-15 material, its channel length is around 400 nm and several times shorter than that of traditional SBA-15 material [32].

As shown in Fig. 4a, the MCM-41 spheres demonstrate perfectly orbicular shape and a spherically symmetric channel distribution [33, 29]. The morphology and particle size of the current MCM-41 material make its channel length 300–400 nm, which is much shorter than that of a conventional MCM-41 material [28]. Such short channel length can benefit achieving high loading capacity [18, 20]. Figure 4b shows that the MCF material is composed of uniformly sized, large spherical cells with the size around 30 nm, being in agreement with that calculated by N_2 adsorption–desorption isotherms (Table 1). These spherical cells are interconnected by uniform windows to create a 3-D channel system, which is good for achieving high loading capacity and reducing pore blocking.

Figure 5 shows the FTIR and UV–Vis DRS spectra of the support materials, lipase LVK-S200 and immobilized lipase catalysts. As shown in Fig. 5a, the spectra of all three support materials show typical characteristics of the IR spectrum of a silica material. Each support material gives a broad band around 1,635 cm^{-1} due to the O–H bending vibrations of adsorbed water. This broad band around 1,635 cm^{-1} can also be identified in the spectra of LVK-S200 and three immobilized catalysts. In the spectra of three immobilized catalysts, the IR bonds at 2,932 cm^{-1} and the bands in the range of 1,368–1,462 cm^{-1} related to the lipase LVK-S200 can be identified, confirming the successful immobilization of the lipase on the support materials. The UV–Vis DRS spectra shown in Fig. 5b suggest the same as FTIR spectra do. No band can be observed in the spectra of the support materials, which are composed of silica. In the spectra of three immobilized catalysts, the bands at 234, 286, and 320 nm can be observed due to the immobilization of LVK-S200 on the support materials.

Table 1 Textural properties of the support materials

Support materials	Channel size (nm)	Specific area ($m^2\ g^{-1}$)	Pore volume ($cm^3\ g^{-1}$)
MCM-41	1.8	1,007	0.81
SBA-15	14.0	750	1.39
MCF	28.2	680	2.46

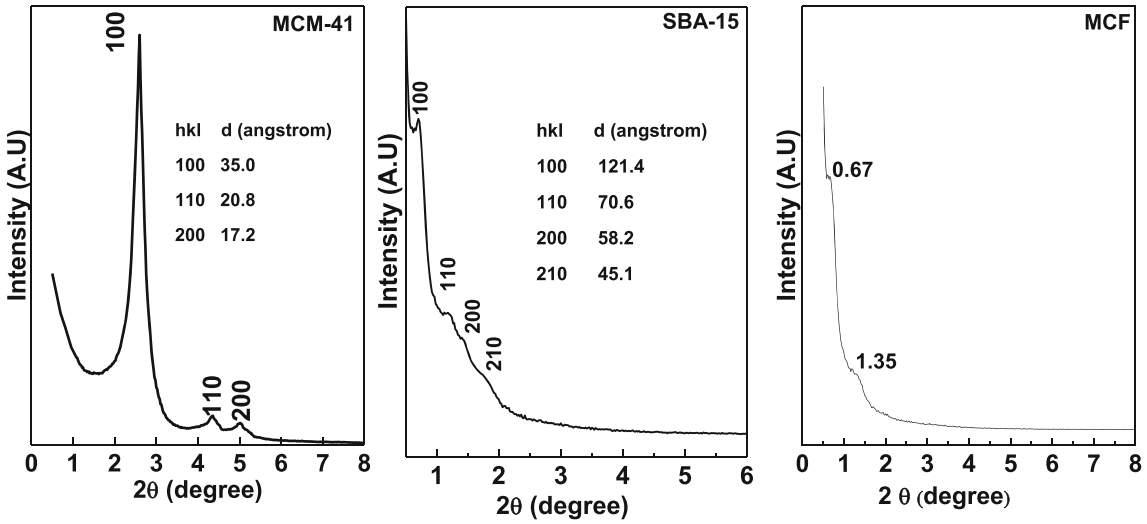

Fig. 2 SXRD patterns of the MCM-41, SBA-15, and MCF support materials

Catalytic Performance of Immobilized Lipase Catalysts

Figure 6 presents the initial specific activity for these immobilized lipase catalysts in the transesterification reactions of POO. The initial specific activity of support lipase catalysts greatly increases while the support material changed from MCM-41 to SBA-15, with a remarkable increase in channel size and channel volume but decrease in specific area. Considering the marked change in the specific area of these three different support materials, the initial specific activity was normalized based on the specific area of each support material. The normalized specific activity also greatly increases while the support material changes from MCM-41 to SBA-15 and then decreases with the change from SBA-15 to MCF. This suggests that big channel size and big channel volume of support material can benefit achieving a high specific activity of immobilized lipase catalysts, but a big specific area cannot. The higher specific activity obtained on LVK/

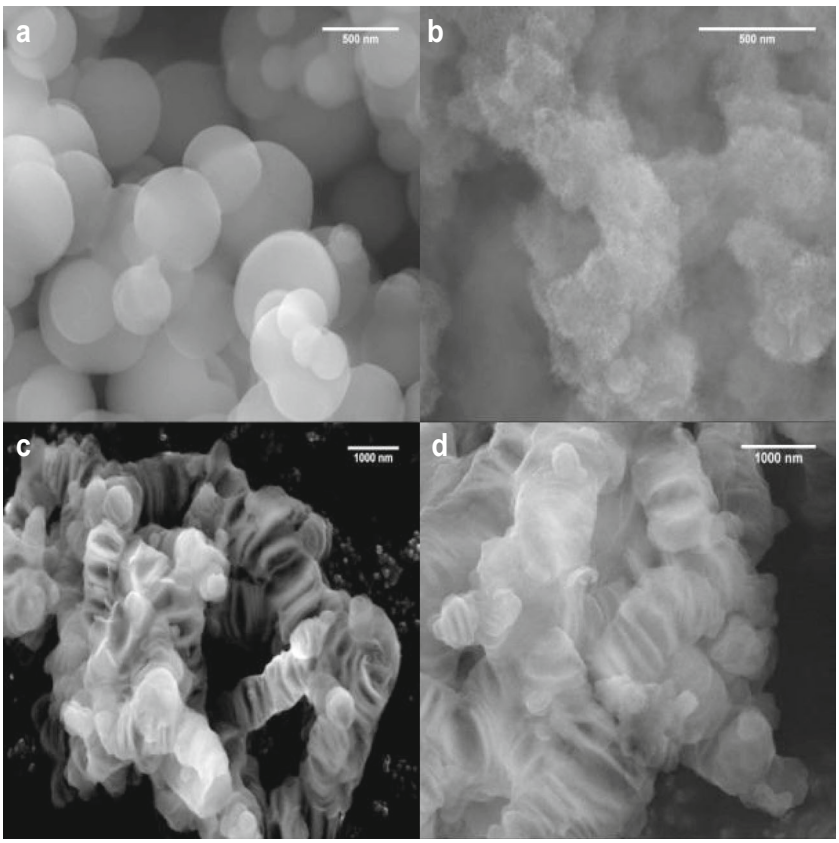

Fig. 3 SEM images of **a** MCM-41, **b** MCF, and **c** SBA-15 materials; **d** HRSEM image of the SBA-15 material

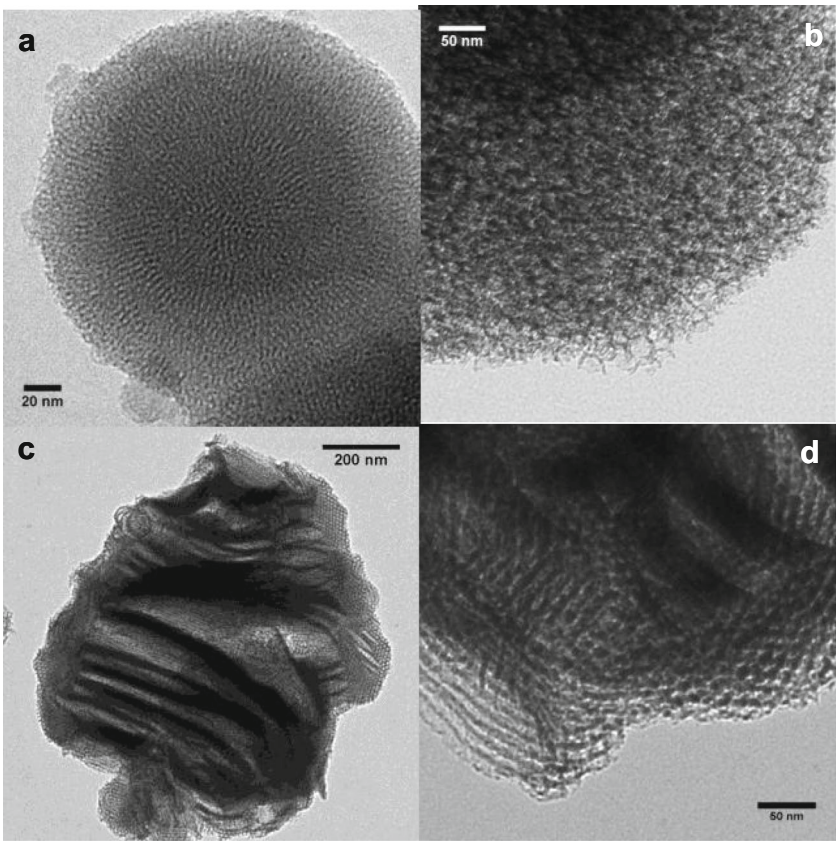

Fig. 4 TEM images of **a** MCM-41, **b** MCF, and **c**, **d** SBA-15 materials

SBA-15 catalyst than LVK/MCM-41 catalyst takes advantage of the non-traditionally big channel size and short channel length of this SBA-15 material in two ways. Firstly, the big channel size and short channel length can exhibit a higher loading capacity owing to reduced pore blocking [34, 20]. Secondly, the big channel size and short channel length can greatly reduce the motion restriction in the transesterification processes [15, 35].

The higher initial specific activity of LVK/SBA-15 than that of LVK/MCM-41 is in agreement with the bigger channel size and shorter channel length of SBA-15 compared to MCM-41. However, in the current work, we found that a further increase in the channel size of MCF does not result in higher initial specific activity but in much lower initial specific activity than SBA-15, although MCF exhibits much bigger channel size and much shorter channel length than

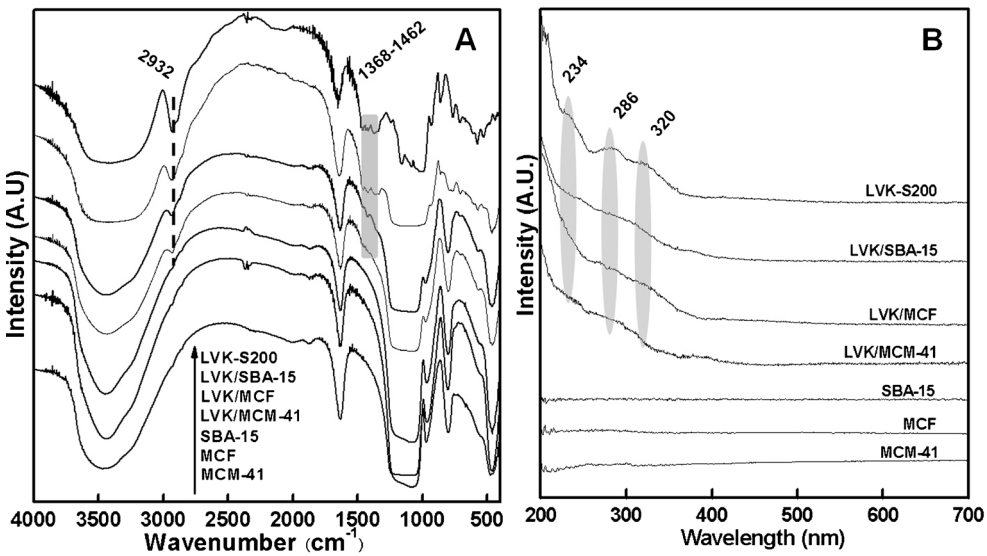

Fig. 5 **a** FTIR and **b** UV–Vis DRS spectra of all support materials, immobilized lipase catalysts, and lipase LVK-S200

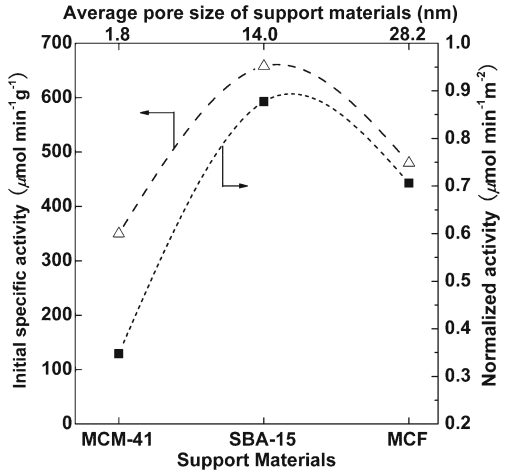

Fig. 6 Initial specific activity of different immobilized lipase catalysts in the transesterification processes of POO

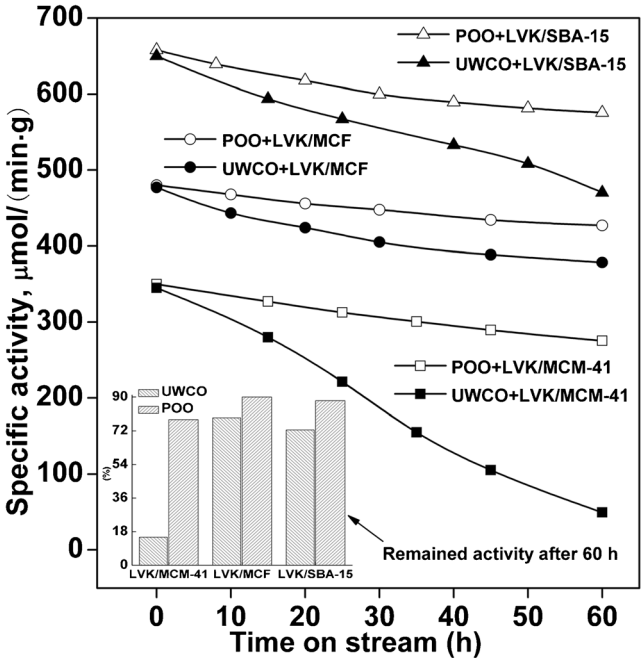

Fig. 7 Catalytic behaviors of immobilized lipase catalysts in the transesterification processes of UWCO and POO. The *inset* demonstrates the remained activity of the immobilized lipase catalysts after a 60-h-long reaction

SBA-15. The normalized specific activity notably decreases with the change of support material from SBA-15 to MCF. This suggests that an optimized channel size should be chosen for the satisfactory adsorption of lipase on mesoporous silica materials, and the SBA-15 material used in current work provides the channel size and pore volume that are far more suitable than those of the other two support materials. The channel size of MCF is big enough for the satisfactory adsorption of lipase inside its nano-channels but also too big to maintain well the adsorbed lipase.

Figure 7 shows the catalytic behaviors of immobilized lipase catalysts in the transesterification processes of UWCO and POO at room temperature. LVK/SBA-15 catalyst exhibits remarkably higher initial specific activity than LVK/MCM-41 and LVK/MCF catalysts, while either POO or UWCO was used as the feedstock of reaction. In a 60-h-long reaction, the yield of FAME to oil up to 80.1 % can be achieved with the use of LVK/SBA-15 catalyst and UWCO as the raw material. The main components in the reaction medium include palmitate methyl, palmitoletic methyl, stearic methyl, oleic methyl, linoleic methyl, and linolenic methyl. Being similar to the initial specific activity for the immobilized lipase catalysts in the transesterification reactions of POO, SBA-15 and MCF result in higher initial specific activity than MCM-41 in the transesterification reactions of UWCO due to their bigger channel size and pore volume than those of MCM-41. Furthermore, LVK/SBA-15 still demonstrates the highest initial specific activity among these immobilized lipase catalysts in the transesterification reactions of UWCO.

In most cases, the processes for biodiesel production require the use of virgin oils with high quality and purity [36]. The UWCO we tested was simply filtrated to remove indissoluble impurities and then put into transesterification processes. In Fig. 7, it can be observed that the specific activity of LVK/MCM-41 catalyst decreases sharply to a very low level (14.2 % of starting value) in the transesterification processes of UWCO due to the motion restriction arising from possible block by UWCO in its small nano-channels. The non-traditional SBA-15 material used in this work has large channel size and short length nano-channels and thus exhibits little suppressant effect on the activity of immobilized LVK-S200 species. In the transesterification processes of UWCO, the LVK/SBA-15 catalyst is very effective at the start of reaction and shows considerable initial activity in comparison with its activity in the transesterification processes of POO. The comparative study on the specific activities of LVK/SBA-15 catalyst for UWCO and POO indicates that the specific activity for UWCO decreases more than that for POO. However, within 60 h, the specific activity of LVK/SBA-15 still remains at a remarkable level (71.8 % of starting value) in the UWCO reaction system.

In the transesterification processes of UWCO catalyzed by LVK/MCF catalyst, its specific activity even remained at a higher level (78.2 % of starting value) than that of LVK/SBA-15 catalyst due to the novel 3-D pore system of MCF. The biggest channel size and novel 3-D pore system of MCF give the LVK/MCF catalyst the best capability to maintain high specific activity among these immobilized lipase catalysts in the transesterification processes of UWCO. However, in the transesterification processes of POO, the remaining level (88.9 % of starting value) of initial specific activity of LVK/SBA-15 catalyst is very close to that (87.4 % of starting value) of the LVK/MCF catalyst. Notably, in the transesterification processes of POO, the specific activity of LVK/MCM-41

catalyst can remain at a high level (76.6 % of starting value) after 60 h. This reflects that big channel size is the key point to keep high specific activity in the transesterification processes of UWCO, because it contains the insoluble matter which can result in blocking of nano-channels of support materials. In the transesterification processes of POO, channel size does not show such distinctive effects on the remaining specific activity.

Conclusion

In summary, three different mesoporous silica materials with various channel sizes and channel structures were prepared and employed to prepare immobilized lipase catalysts for the catalytic transesterification processes of UWCO to biodiesel at room temperature. It is found that an optimized channel size of support material is the key point to achieve high initial specific activities of immobilized lipase catalysts and maintain the high specific activity in the transesterification processes of UWCO. A SBA-15 material, which contains nano-channels 14 nm in pore size and 400 nm in channel length, demonstrates the best capacity of lipase LVK S200. The LVK/SBA-15 catalyst shows much better catalytic behavior than the LVK/MCF and LVK/MCM-41 catalysts. After a 60-h-long reaction, the yield of FAME to oil up to 80.1 % as well as a specific activity up to 71.8 % of the starting value can be achieved using the LVK/SBA-15 catalyst.

Acknowledgments The authors are grateful for the National Natural Science Foundation of China (NSFC U1362105, 21306233), the Science Research Project (KJ130729, KJ130702) of Chongqing Education Commission, the Chongqing Science and Technology Foundation (cstc2013jcyjA50007, cstc2014yykfB90002, jcsf121-2012-02-1), and the Chongqing 100 leading scientists promotion project.

References

1. Kulkarni MG, Dalai AK (2006) Waste cooking oil an economical source for biodiesel: a review. Ind Eng Chem Res 45:2901–2913
2. Phan AN, Phan TM (2008) Biodiesel production from waste cooking oils. Fuel 87:3490–3496
3. Sivaramakrishnan R, Muthukumar K (2012) Production of methyl ester from *Oedogonium* sp. oil using immobilized isolated novel *Bacillus* sp. lipase. Energy Fuels 26:6387–6392
4. Ragit SS, Mohapatra SK, Kundu K, Gill P (2011) Optimization of neem methyl ester from transesterification process and fuel characterization as a diesel substitute. Biomass Bioenergy 35:1138–1144
5. Du ZX, Tang Z, Wang HJ, Zeng JL, Chen YF, Min EZ (2013) Research and development of a sub-critical methanol alcoholysis process for producing biodiesel using waste oils and fats. Chin J Catal 34:101–115
6. Zhang Y, Dubé MA, Mclean DD, Kates M (2003) Biodiesel production from waste cooking oil: 1. Process design and technological assessment. Bioresour Technol 89:1–16
7. Maddikeri GL, Pandi AB, Gogate PR (2012) Intensification approaches for biodiesel synthesis from waste cooking oil: a review. Ind Eng Chem Res 51:14610–14628
8. Srilatha K, Issariyakul T, Lingaiah N, Prasad PSS, Kozinski J, Dalai AK (2010) Efficient esterification and transesterification of used cooking oil using 12-tungstophosphoric acid (TPA)/Nb_2O_5 catalyst. Energy Fuels 24:4748–4755
9. Ahmad AL, Mat NHY, Derek CJC, Lim JK (2011) Microalgae as a sustainable energy source for biodiesel production: a review. Renewable Sustainable Energy Rev 15:584–593
10. Zhang Y, Dubé MA, Mclean DD, Kates M (2003) Biodiesel production from waste cooking oil: 2. Economic assessment and sensitivity analysis. Bioresour Technol 90:229–240
11. Wu WH, Foglia TA, Marmer WN, Phillips JG (1999) Optimizing production of ethyl esters of grease using 95 % ethanol by response surface methodology. J Am Oil Chem Soc 76:517–521
12. Hsu A, Jones KC, Foglia TA, Marmer WN (2004) Continuous production of ethyl esters of grease using an immobilized lipase. J Am Oil Chem Soc 81:749–752
13. Véras IC, Silva FAL, Ferrão-Gonzales AD, Moreau VH (2011) One-step enzymatic production of fatty acid ethyl ester from high-acidity waste feedstocks in solvent-free media. Bioresour Technol 102: 9653–9658
14. Hsu A, Jones KC, Marmer WN (2001) Production of alkyl esters from tallow and grease using lipase immobilized in a phyllosilicate sol–gel. J Am Oil Chem Soc 78:585–588
15. Shen Y, Zhang HD, Zheng XX, Zhang XM, Chen LG (2012) Production of biodiesel from waste cooking oil by lipase immobilized in mesoporous cellular foam support. CIESC J 63: 1888–1892
16. Noureddini H, Gao X, Philkana R (2005) Immobilized *Pseudomonas cepacia* lipase for biodiesel fuel production from soybean oil. Bioresour Technol 96:769–777
17. Hartmann M (2008) Ordered mesoporous materials for bioadsorption and biocatalysis. Chem Mater 17:4577–4593
18. Hudson S, Magner E, Cooney J, Hodnett BK (2005) Methodology for the immobilization of enzymes onto mesoporous materials. J Phys Chem B 109:19496–19506
19. Diaz JF, Balkus JKJ (1996) Enzyme immobilization in MCM-41 molecular sieve. J Mol Catal B Enzym 115–126
20. Hudson S, Cooney J, Magner E (2008) Proteins in mesoporous silicates. Angew Chem Int Ed 47:8582–8594
21. Katiyar A, Ji L, Smirniotis P, Pinto NG (2005) Protein adsorption on the mesoporous molecular sieve silicate SBA-15: effects of pH and pore size. J Chromatogr A 1069:119–126
22. Kalantari M, Kazemeini M, Tabandeh F, Arpanaei A (2012) Lipase immobilisation on magnetic silica nanocomposite particles: effects of the silica structure on properties of the immobilised enzyme. J Mater Chem 22:8385–8393
23. Gao F, Ma GH (2012) Effects of microenvironment on supported enzymes. Top Catal 55:1114–1123
24. Hanefeld U, Gardossi L, Magner E (2009) Understanding enzyme immobilization. Chem Soc Rev 38:453–468
25. Zhang HD, Shen Y (2012) Straight chain alkane-assisted synthesis of mesoporous silica. Mater Lett 75:183–185
26. Zhang HD, Wang YM, Lü K, Hensen EJM, Zhang L, Zhang WH, Abbenhuis HCL, Li C, van Santen RA (2012) Hierarchical fabrication of silica cocoon with hexagonally ordered channel constructed wall via an emulsion-assisted process. Micropor Mesopor Mater 150: 90–95
27. Zhao D, Feng J, Huo QS, Melosh N, Fredrickson GH, Chmelka BF, Stucky GD (1998) Triblock copolymer syntheses of mesoporous silica with periodic 50 to 300 angstrom pores. Sci 279:548–552
28. Wan Y, Zhao DY (2007) On the controllable soft-templating approach to mesoporous silicates. Chem Rev 107:2821–2860

29. Pauwels B, Tendeloo GV, Thoelen C, Rhijn WV, Jacobs PA (2001) Structure determination of spherical MCM-41 particles. Adv Mater 13:1317–1320
30. Lebedev OI, Tendeloo G, Collart VO, Cool P, Vansant EF (2004) Structure and microstructure of nanoscale mesoporous silica spheres. Solid State Sci 6:489–498
31. Grün M, Unger KK, Matsumoto A, Tsutsumi K (1999) Novel pathways for the preparation of mesoporous MCM-41 materials: control of porosity and morphology. Micropor Mesopor Mater 27:207–216
32. Zhao DY, Huo QS, Feng J, Chmelka BF, Stucky GD (1998) Nonionic triblock and star diblock copolymer and oligomeric surfactant syntheses of highly ordered, hydrothermally stable, mesoporous silica structures. J Am Chem Soc 120:6024–6036
33. Tendeloo GV, Lebedev OI, Collart O, Cool P, Vansant EF (2003) Structure of nanoscale mesoporous silica spheres? J Phys: Condensed Matter 15:S3037–3046
34. Fan J, Lei J, Wang L, Yu C, Tu B, Zhao DY (2003) Rapid and high-capacity immobilization of enzymes based on mesoporous silicas with controlled morphologies. Chem Commun 34:2140–2141
35. Zhang HD, Wang YM, Zhang L, Gerritsen G, Abbenhuis HCL, van Santen RA, Li C (2008) Enantioselective epoxidation of β-methylstyrene catalyzed by immobilized Mn(salen) catalysts in different mesoporous silica supports. J Catal 256:226–236
36. McNeff CV, McNeff LC, Yan BW, Nowlan DT, Rasmussen M, Gyberg AE, Krohn BJ, Fedie RL, Hoye TR (2008) A continuous catalytic system for biodiesel production. Appl Catal A Gen 343:39–49